



Heat capacities and thermodynamic functions of D-ribose and D-mannose

Siyu Wang^{1,2} · Youyou Zhang^{1,2} · Jian Zhang¹ · Shaoxu Wang² · Zhicheng Tan¹ · Quan Shi¹

Received: 10 November 2017 / Accepted: 24 February 2018 / Published online: 8 March 2018
© Akadémiai Kiadó, Budapest, Hungary 2018

Abstract

The heat capacities of D-ribose and D-mannose have been studied over the temperature range from 1.9 to 440 K for the first time using a combination of Quantum Design Physical Property Measurement System and a differential scanning calorimeter. The purity, crystal phase and thermal stability of these two compounds have been characterized using HPLC, XRD and TG–DTA techniques, respectively. The heat capacities of D-Mannose have been found to be larger than those of D-ribose due to its larger molecular weight, and the solid–liquid transition due to the sample melting has also been detected in the heat capacity curve. The heat capacities of these two compounds have been fitted to a series of theoretical models and empirical equations in the entire experimental temperature region, and the corresponding thermodynamic functions have been derived based on the curve fitting in the temperature range from 0 to 440 K. Moreover, the phase transition enthalpy and melting temperature of these two compounds have also been determined from the heat flows obtained in DSC measurements.

Keywords D-Ribose · D-Mannose · Heat capacity · Thermodynamic functions · Physical property measurement system · DSC

Introduction

D-Ribose and D-mannose are important carbohydrates which have been widely used in agricultural production, food industry, pharmaceutical industry, and medical treatment [1–5]. D-Ribose (C₅H₁₀O₅) and D-mannose (C₆H₁₂O₆) are common biological monosaccharides existing in living cells as energy sources. D-Ribose, belonging to reducing pentoses, exists in living organisms not only as the main

component of the nucleotide but also as raw materials of physiological macromolecules such as adenosine triphosphate (ATP) and adenosine diphosphate (ADP). At room temperature, D-ribose is usually white orthorhombic crystal or crystalline powder. D-Mannose is an isomeride of glucose, containing six carbon atoms forming a six-membered ring, which can be utilized to synthesize glycoproteins in plant cell wall. D-Mannose is mainly present in the form of free-state oligosaccharides in fruit epidermis cell wall and in the form of polysaccharides in yeast and red algae.

The studies of D-ribose and D-mannose in the last 40 years have mainly focused on the synthesis of new derivatives [6], structure determination [7, 8], and biological activity [9–11]. However, the studies of thermodynamic properties of these two compounds are needed for better understanding their roles in synthesis mechanism, structure formation or transition, and biological induction from a view of thermodynamics.

Wilhoit [12] reported the standard enthalpy of combustion and the standard enthalpy of formation for D-ribose. Colbert et al. [13] determined the enthalpy of combustion for D-ribose. Banipal et al. [14] measured the partial molar heat capacities and volumes of D-ribose and D-mannose in

Electronic supplementary material The online version of this article (<https://doi.org/10.1007/s10973-018-7128-8>) contains supplementary material, which is available to authorized users.

✉ Quan Shi
shiquan@dicp.ac.cn

¹ Thermochemistry Laboratory, Dalian Institute of Chemical Physics, Chinese Academy of Science, Liaoning Province Key Laboratory of Thermochemistry for Energy and Materials, Dalian National Laboratory for Clean Energy, Dalian 116023, People's Republic of China

² College of Environmental Science and Engineering, Dalian Jiaotong University, Dalian 116028, People's Republic of China

water at 298.15, 308.15 and 318.15 K and in NaCl solution at 298.15 K using a Picker flow microcalorimeter, and calculated the partial molar expansion coefficients, isothermal compressibilities, excess partial molecular volumes and partial molar heat capacity coefficients. Robert et al. [15] studied the thermodynamic and transport properties of some carbohydrates at 298.15 K. Saskia et al. [16] discussed the apparent molar heat capacities of some carbohydrates in aqueous solutions versus the molality of carbohydrates at 298.15 K. Zhuo et al. [8] studied the system of electrolyte (NaCl, NaBr and NaI)-monosaccharide(D-Ribose and D-Mannose)-water solutions at 298.15 K and calculated the apparent molar volumes and evaluated the infinite dilution apparent molar volumes of the saccharides and electrolytes. Alberty reported the thermodynamic properties and calculated the standard Gibbs energies of formation and standard enthalpies of formation for D-ribose crystals [17].

However, the heat capacities and the related thermodynamic functions of D-ribose and D-mannose have not been reported especially in a wide temperature region covering their solid–liquid transition. In this work, we have measured the heat capacities of D-ribose and D-mannose in the temperature range from 1.9 to 440 K using the combination of a Physical Property Measurement System and a differential scanning calorimeter. The measured heat capacities have been fitted to a series of theoretical models and empirical equations, and consequently, the corresponding thermodynamic functions have been calculated based on the fitting parameters.

Experimental

The D-mannose and D-ribose samples used in the calorimetric measurements were commercially provided by J & K Scientific Ltd, and their molecular structure and sample information are listed in Fig. 1 and Table 1, respectively. The sample purity was further confirmed by means of HPLC method on a HPAEC system consisting of a Dionex Bio-LC gradient pump with GM-3 (4 mm) gradient mixer, CarboPac PA-10 column (4 × 250 mm), and an

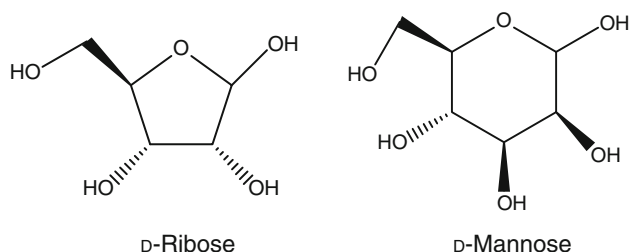


Fig. 1 The molecular structures of D-ribose and D-mannose

electrochemical detector using AgCl as reference electrode. The waveform was carbohydrates (standard Quad) and the following pulse potentials were used for the detection: $t = 0$ s, $E = 0.10$ v; $t = 0.20$ s, $E = 0.10$ v; $t = 0.40$ s, $E = 0.10$ v; $t = 0.41$ s, $E = -2.00$ v; $t = 0.42$ s, $E = -2.00$ v; $t = 0.43$ s, $E = 0.60$ v; $t = 0.44$ s, $E = -0.10$ v; $t = 0.50$ s, $E = -0.10$ v. The sample injection volume was 20 μ L with the column oven temperature maintained at 303 K, while the reference standards were resolved by 18 mM NaOH isocratic elution at a flow rate of 0.5 mL min^{-1} over a 40 min time interval. The HPLC results listed in Table 1 indicating the mass fraction purity for both compounds to be better than 99%.

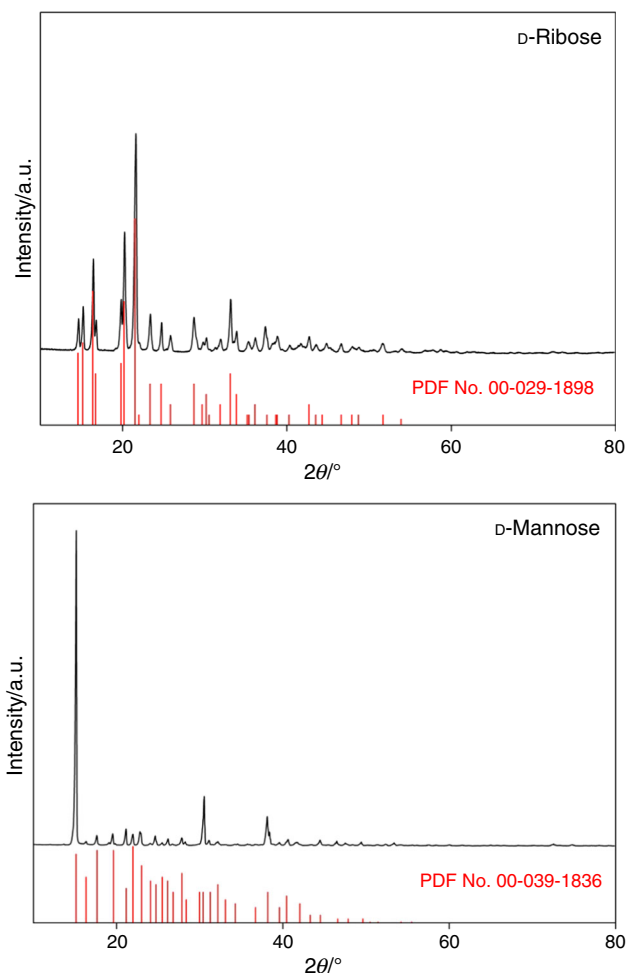
The phase purity was examined using a powder X-ray diffraction instrument with a Cu Ka radiation (0.15418 nm) (PANalytical Co. X'pert PRO, Netherlands) operated under a voltage of 40 kV and a current of 40 mA. The XRD patterns collected for these two compounds are presented in Fig. 2. It can be seen that the diffraction peaks of D-ribose and D-mannose are well consistent with the standard patterns (PDF card No. 00-029-1898) and (PDF card No. 00-039-1836), respectively, from International Centre for Diffraction Data, indicating that these samples measured in this work are phase pure. The thermal stability of D-mannose and D-ribose was inspected using a thermogravimetric analyzer (SETSYS 16/18, SETARAM Co., France) from room temperature to 1073 K with a heating rate of 10 K min^{-1} and a high-purity Nitrogen atmosphere. The sample mass used in the measurement is 0.02313 g for D-ribose and 0.02228 g for D-mannose.

The low-temperature heat capacities were measured using a Quantum Design Physical Property Measurement System (PPMS) with a logarithmic spacing from 1.9 to 100 K and a 10 K temperature interval from 100 to 300 K. The accuracy of the PPMS heat capacity measurement was estimated, by measuring the heat capacities of a high-purity copper pellet, α -Al₂O₃ (SRM720) and benzoic acid (SRM39j), and comparing the measured data to the standard values, to be $\pm 3\%$ in the temperature region from 1.9 to 20 K and $\pm 1\%$ from 20 to 300 K [18]. The powdered sample was prepared into a pellet to meet the PPMS requirement using a method developed by Shi et al., and the detailed sample preparation process and measurement procedure can be found in previous publications [19, 20]. The sample amounts used in the measurements were 0.01152 and 0.00880 g for D-ribose and D-mannose, respectively.

The heat capacities of D-ribose and D-mannose in the melting region were measured in the temperature range from 188 to 440 K using a heat-flux differential scanning calorimeter (Discovery DSC2500 from TA Instruments). The temperature calibration was performed by determining the melting temperature of indium. The extrapolated onset

Table 1 Information of the studied samples used in this study

Chemical name	CAS no.	Formula	Source	$X^a/\%$	$X_c^b/\%$
D-Ribose	50-69-1	$C_5H_{10}O_5$	J & K Scientific	99	99.73
D-Mannose	3458-28-4	$C_6H_{12}O_6$	J & K Scientific	99	99.57

^aThe mass fraction purity provided by the suppliers^bThe mass fraction purity measured by HPLC**Fig. 2** The XRD patterns of D-ribose and D-mannose

of indium was compared to the known melting point, and the difference was recorded for temperature calibration. The uncertainty for the enthalpy measurement in the DSC instrument is within $\pm 3\%$. The DSC heat capacity measurement accuracy was estimated, by measuring the heat capacity of $\alpha\text{-Al}_2\text{O}_3$ (SRM720), to be within $\pm 3\%$ in the temperature range from $T = 183$ to 673 K. The temperature intervals in the measurement were set to be 1 K in non-transition region and 0.1 K in transition region with a heating rate of 10 K min^{-1} and a high-purity nitrogen purge gas flow rate of 50 cm^3 min^{-1} . The sample amounts used in the measurements were 0.0937 and 0.0767 g for D-ribose and D-mannose, respectively.

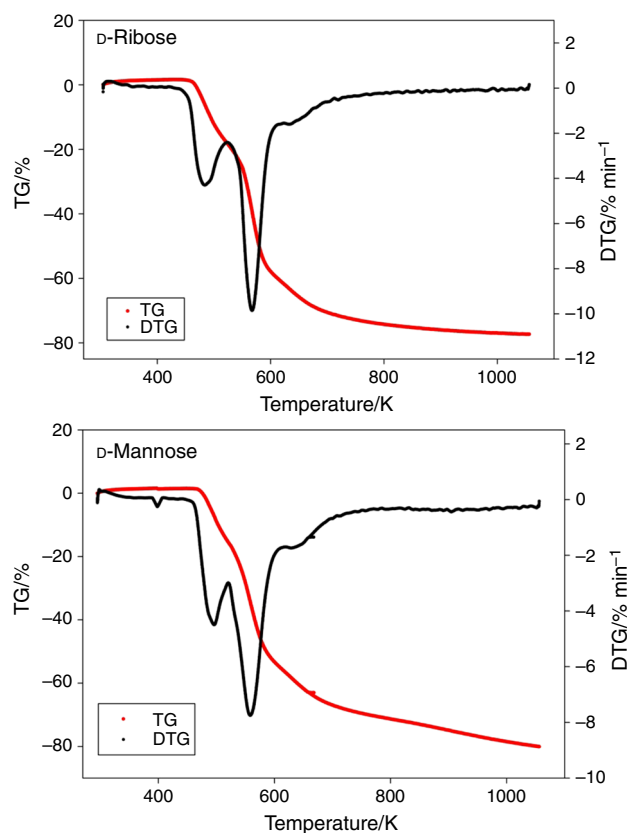
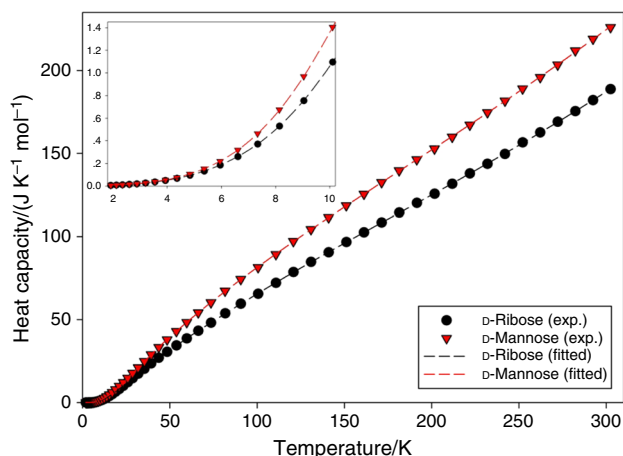
**Fig. 3** TG-DTG curves of D-ribose and D-mannose**Fig. 4** Plot of the experimental and fitted heat capacities of D-ribose and D-mannose measured with PPMS

Table 2 Experimental molar heat capacities $C_{p,m}^{\theta}$ at constant pressure ($p = 1.2$ mPa) for D-ribose and D-mannose from $T = 1.9$ to 300 K

D-Ribose				D-Mannose			
T/K	$C_{p,m}^{\theta} / J K^{-1} mol^{-1}$	T/K	$C_{p,m}^{\theta} / J K^{-1} mol^{-1}$	T/K	$C_{p,m}^{\theta} / J K^{-1} mol^{-1}$	T/K	$C_{p,m}^{\theta} / J K^{-1} mol^{-1}$
1.917	5.9792E-03	43.671	26.9773	1.920	6.5595E-03	43.671	33.3020
2.125	7.9104E-03	48.470	30.5504	2.125	8.6864E-03	48.453	37.8812
2.351	1.0595E-02	53.801	34.4268	2.350	1.1480E-02	53.793	42.9093
2.603	1.4237E-02	59.722	38.6744	2.600	1.5311E-02	59.704	48.3671
2.883	1.9295E-02	66.301	43.2532	2.881	2.0664E-02	66.270	54.1912
3.201	2.6386E-02	73.616	48.1122	3.199	2.8485E-02	73.588	60.2944
3.547	3.5886E-02	81.731	53.7634	3.545	3.8869E-02	81.692	67.2756
3.934	4.9120E-02	90.709	59.5858	3.931	5.3581E-02	90.672	74.3161
4.362	6.7830E-02	100.652	65.5868	4.357	7.4953E-02	100.613	81.4399
4.839	9.4752E-02	110.835	72.1571	4.835	1.0662E-01	110.790	89.3073
5.369	1.3164E-01	120.849	78.6938	5.364	1.5168E-01	120.777	97.1964
5.956	1.8446E-01	130.920	84.8083	5.951	2.1927E-01	130.878	104.3478
6.609	2.5992E-01	141.011	90.5711	6.604	3.1790E-01	141.003	111.5021
7.338	3.7063E-01	151.156	96.7371	7.331	4.6358E-01	151.110	118.6105
8.145	5.2970E-01	161.242	102.5664	8.138	6.7471E-01	161.206	125.5415
9.041	7.5397E-01	171.354	108.4965	9.035	9.6839E-01	171.305	132.5274
10.106	1.0949	181.463	114.4261	10.099	1.4038	181.394	139.6743
11.213	1.5320	191.564	120.2172	11.210	1.9541	191.496	146.3444
12.447	2.1186	201.684	125.6764	12.446	2.6785	201.616	152.8175
13.817	2.8784	211.792	131.7060	13.815	3.6000	211.751	159.9247
15.356	3.8489	221.893	137.9524	15.352	4.7449	221.846	167.1653
17.040	5.0291	231.981	143.7220	17.040	6.1617	231.953	174.6706
18.925	6.4629	241.982	149.6728	18.923	7.8570	241.965	181.6544
21.016	8.1380	252.136	156.6587	21.011	9.8426	252.111	188.9756
23.339	10.0615	262.204	162.6446	23.338	12.1553	262.181	195.8444
25.910	12.2553	272.233	169.1162	25.910	14.7816	272.205	203.4133
28.737	14.6804	282.300	175.4816	28.730	17.7607	282.276	211.9503
31.906	17.4218	292.446	182.1156	31.900	21.1015	292.422	219.0382
35.430	20.3577	302.490	188.7672	35.422	24.8292	302.447	225.9912
39.344	23.5906			39.332	28.9184		

The estimated standard uncertainties in the pressure p and temperature T are $u(p) = 0.10$ mPa, and $u(T) = 0.01$ K ($2 < T/K < 20$), $u(T) = 0.02$ K ($20 < T/K < 100$), and $u(T) = 0.05$ K ($100 < T/K < 300$). The expanded uncertainties at approximately 95 percent confidence limits in the values of $C_{p,m}^{\theta}$ are $U(C_{p,m}^{\theta}) = 0.03 \cdot C_{p,m}^{\theta}$ from $T = 1.9$ to 20 K, $U(C_{p,m}^{\theta}) = 0.01 \cdot C_{p,m}^{\theta}$ from $T = 20$ to 220 K and $U(C_{p,m}^{\theta}) = 0.025 \cdot C_{p,m}^{\theta}$ from $T = 220$ to 400 K

Results and discussion

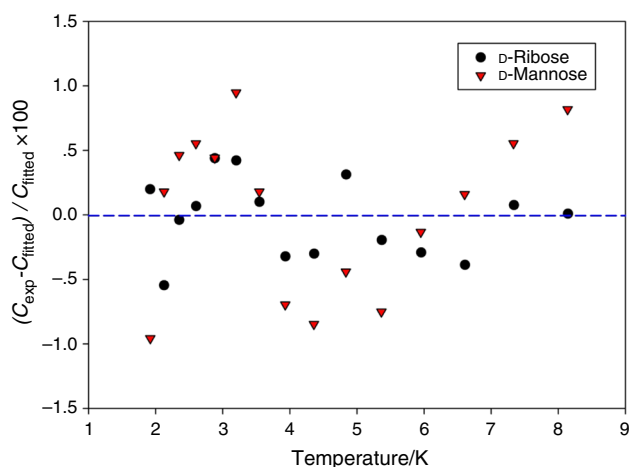
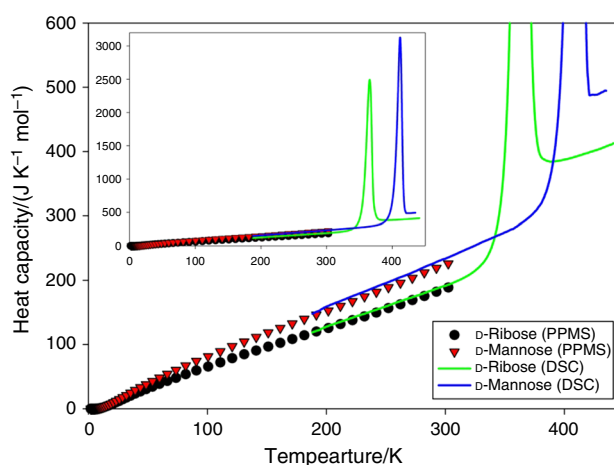
TG analysis

The thermal stability of D-ribose and D-mannose was evaluated using the TG measurement, and the TG curve is presented in Fig. 3. It can be seen from Fig. 3 that these two compounds both behave a thermal decomposition process with a three-step weight loss in the entire temperature region. D-ribose exhibits a percent weight loss of 19.75, 42.7 and 9.92% in the temperature region from 451

to 523, 523 to 618 and 618 to 705 K, respectively. D-mannose appears to decompose at a little higher temperature with percent weight loss of 15.27, 40.51 and 12.1% in the region from 462 to 519, 519 to 611 and 611 to 708 K, respectively. Based on these results, it can be concluded that both D-ribose and D-mannose are thermally stable in the heat capacity measurement region below 440 K.

Table 3 Fitting parameters of heat capacities of D-ribose and D-mannose

Parameter	D-ribose	D-mannose
Low T fits		
$\gamma/J \text{ mol}^{-1} \text{ K}^{-2}$	3.1341E-04	8.3889E-04
$B_3/J \text{ mol}^{-1} \text{ K}^{-4}$	7.4204E-04	6.6607E-04
$B_5/J \text{ mol}^{-1} \text{ K}^{-6}$	3.3197E-06	1.1607E-05
$B_7/J \text{ mol}^{-1} \text{ K}^{-8}$		-4.6956E-08
%RMS	0.841	0.586
Range/K	0-6.50	0-9.28
Mid T fits		
$A_0/J \text{ mol}^{-1} \text{ K}^{-1}$	-5.8598E-01	-3.1881E-01
$A_1/J \text{ mol}^{-1} \text{ K}^{-2}$	3.9471E-01	2.7458E-01
$A_2/J \text{ mol}^{-1} \text{ K}^{-3}$	-1.0030E-01	-8.5503E-02
$A_3/J \text{ mol}^{-1} \text{ K}^{-4}$	1.2541E-02	1.2490E-02
$A_4/J \text{ mol}^{-1} \text{ K}^{-5}$	-6.2613E-04	-6.5940E-04
$A_5/J \text{ mol}^{-1} \text{ K}^{-6}$	1.6846E-05	1.8543E-05
$A_6/J \text{ mol}^{-1} \text{ K}^{-7}$	-2.5617E-07	-2.9309E-07
$A_7/J \text{ mol}^{-1} \text{ K}^{-8}$	2.0697E-09	2.4479E-09
$A_8/J \text{ mol}^{-1} \text{ K}^{-9}$	-6.8982E-12	-8.3902E-12
%RMS	0.221	0.268
Range/K	6.50-54.60	9.28-54.3
High T fits		
n_D/mol	1.6005E+00	1.8888E+00
Θ_D/K	1.8638E+02	2.0508E+02
n_E/mol	1.4533E+00	1.2440E+00
Θ_E/K	4.4472E+02	4.5357E+02
$a/J \text{ mol}^{-1} \text{ K}^{-2}$	1.5035E-01	2.8388E-01
$b/J \text{ mol}^{-1} \text{ K}^{-3}$	8.0744E-04	7.5245E-04
%RMS	0.174	0.208
Range/K	54.60-302	54.3-302

**Fig. 5** Plot of deviations ($100 \times (C_{\text{exp}} - C_{\text{fitted}}) / C_{\text{fitted}}$) of the experimental heat capacities from the fitted values against temperatures for D-ribose and D-mannose below 10 K**Fig. 6** Plot of the experimental heat capacities of D-ribose and D-mannose within the temperature range from 1.9 to 440 K from DSC and PPMS measurements

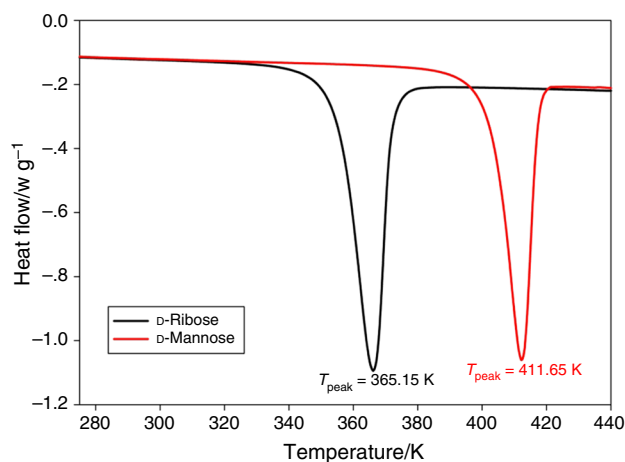


Fig. 7 Plot of the experimental heat flows for D-ribose and D-mannose from DSC measurement

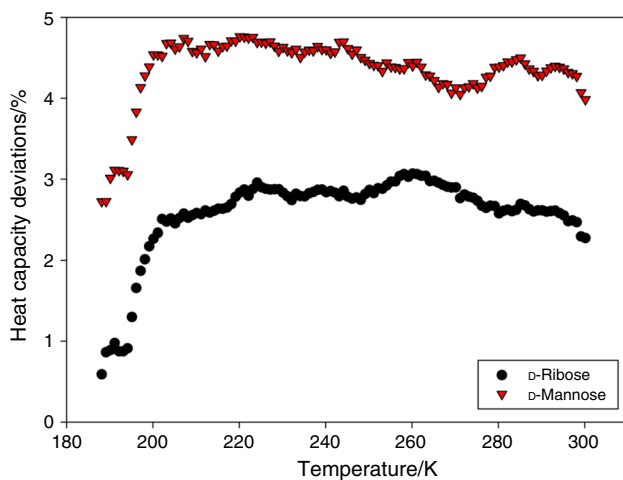


Fig. 8 Plot of deviations ($100 \times (C_{\text{dsc}} - C_{\text{ppms}}) / C_{\text{ppms}}$) of PPMS heat capacities from those of DSC in the region of $T = 180$ to 300 K

PPMS heat capacities

The heat capacities of D-ribose and D-mannose measured using the PPMS in the temperature range from 1.9 to 300 K are plotted in Fig. 4 and listed in Table 2. It is clearly seen that the heat capacities of both compounds increase with the temperature increasing, and no phase transition, decomposition or other thermal anomalies can be detected in this temperature region. Also, D-mannose has a larger heat capacity than that of D-ribose due to its larger molecular weight.

In order to calculate the thermodynamic functions, the measured heat capacities of these two compounds were fitted to a series of empirical and theoretical models in the related temperature region. The heat capacities below 10 K were fitted to the theoretical model below [21],

$$C_{p,m}^o = \gamma T + B_3 T^3 + B_5 T^5 + B_7 T^7 \quad (1)$$

where the linear term represents the contribution from defects and oxygen vacancies in insulating materials, and the odd power terms in temperature represent the contribution from lattice vibration. The fitting parameters from Eq. (1) are listed in Table 3, and the corresponding percent fitting deviation curve is presented in Fig. 5. It can be seen the percent root-mean-square deviation (%RMS) and fitting deviation are within 0.841 and $\pm 1\%$, respectively, indicating that the theoretical model of Eq. (1) could exactly express the heat capacity data of these two compounds below 10 K.

In the middle temperature range of 10–55 K, the heat capacities were fitted to the following polynomial function [22],

$$C_{p,m}^o = A_0 + A_1 T + A_2 T^2 + A_3 T^3 + A_4 T^4 + A_5 T^5 + A_6 T^6 + A_7 T^7 + A_8 T^8 + A_9 T^9 \quad (2)$$

As for the high-temperature region above 50 K, the heat capacities were fitted to a combination of Debye and Einstein function,

$$C_{p,m}^o = n_D D(\theta_D) + n_E E(\theta_E) + aT + bT^2 \quad (3)$$

where θ_D and θ_E are Debye and Einstein temperatures, $D(\theta_D)$ and $E(\theta_E)$ are Debye and Einstein functions, and n_D and n_E are Debye and Einstein parameters, respectively, and the term of $(aT + bT^2)$ is used for the correction of $(C_V - C_p)$ [23].

All the fitting parameters and %RMS in the corresponding temperature regions are listed in Table 3, and the fitted heat capacities using these parameters are plotted as dashed lines in Fig. 4. The fitting %RMS are 0.841, 0.221, and 0.174 for D-ribose, and 0.586, 0.268, and 0.208 for D-mannose in low-, middle- and high-temperature region, respectively, indicating that these fits can be representative of the measured heat capacity data.

DSC heat capacities

To further study the thermodynamic property at higher temperatures, the heat capacities of D-ribose and D-mannose were measured using the DSC in the temperature range from 180 K up to 440 K. The measurement results are shown in Fig. 6, and the corresponding heat capacity data are provided in Supporting Information (SI). The heat capacities measured by PPMS are also shown in Fig. 6 to compare with the DSC data in the overlapping temperature region. It can be seen in the heat capacity curve that both compounds behave a solid–liquid transition in this temperature region. The heat flows recorded in the DSC measurements are presented in Fig. 7, and the melting onset temperature, peak temperature and transition

Table 4 Fitting parameters in solid–liquid transition region for the experimental molar heat capacity of D-ribose and D-mannose measured by DSC

Parameter	D-ribose	D-mannose
Solid phase fits		
$A_0/\text{J mol}^{-1} \text{K}^{-1}$	4.0406E+05	4.0630E+04
$A_1/\text{J mol}^{-1} \text{K}^{-2}$	−1.3081E+04	−1.3572E+03
$A_2/\text{J mol}^{-1} \text{K}^{-3}$	1.8425E+02	1.9476E+01
$A_3/\text{J mol}^{-1} \text{K}^{-4}$	−1.4747E+00	−1.5699E−01
$A_4/\text{J mol}^{-1} \text{K}^{-5}$	7.3395E−03	7.7969E−04
$A_5/\text{J mol}^{-1} \text{K}^{-6}$	−2.3263E−05	−2.4472E−06
$A_6/\text{J mol}^{-1} \text{K}^{-7}$	4.5873E−08	4.7466E−09
$A_7/\text{J mol}^{-1} \text{K}^{-8}$	−5.1468E−11	−5.2069E−12
$A_8/\text{J mol}^{-1} \text{K}^{-9}$	2.5162E−14	2.4754E−15
%RMS	0.111	0.128
Range/K	300–337.15	300–382.15
Liquid phase fits		
$A_0/\text{J mol}^{-1} \text{K}^{-1}$	4.6665E+06	7.6506E+03
$A_1/\text{J mol}^{-1} \text{K}^{-2}$	−5.6079E+04	−3.4063E+01
$A_2/\text{J mol}^{-1} \text{K}^{-3}$	2.6948E+02	4.0389E−02
$A_3/\text{J mol}^{-1} \text{K}^{-4}$	−6.4721E−01	
$A_4/\text{J mol}^{-1} \text{K}^{-5}$	7.7688E−04	
$A_5/\text{J mol}^{-1} \text{K}^{-6}$	−3.7285E−07	
%RMS	0.092	0.086
Range/K	379.15–440	421.15–440

enthalpy could be determined to be 355.27, 366.23 and 26.02 kJ mol^{−1} for D-ribose, and 403.09, 412.26 and 26.41 kJ mol^{−1} for D-mannose.

Also, it can be noted that the DSC data is a little larger than the PPMS data, and their deviations are determined in Fig. 8 to be within 3 and 5% for D-ribose and D-mannose, respectively. These deviations are likely reasonable since these two sets of data were measured using two different calorimetric methods, and also the DSC measurement uncertainties may be easily affected by many factors, such as sample amounts, morphologies, conductivities, as well as experimental conditions [24]. In order to avoid the effect of these deviations on the thermodynamic function calculation over the entire temperature region, we have scaled the DSC heat capacity data by multiplying a scaling factor to match the PPMS data. The scaling factors are 0.975 and 0.961 for D-ribose and D-mannose, respectively. The scaled DSC heat capacities in the solid and liquid phase temperature region were fitted to a polynomial function of Eq. (2), and the data in the melting transition region were fitted using a spline fitting method. The fitting parameters and corresponding RMS% are listed in Table 4.

Thermodynamic functions

Based on the heat capacity fitting parameters listed in Tables 3 and 4, the thermodynamic functions of D-ribose

and D-mannose have been calculated using the thermodynamic relationship of Eqs. (4) and (5) in the temperature range from 0 to 440 K, and the calculated results are listed in Table 5. The standard molar heat capacity, entropy and enthalpy at 298.15 K and 0.1 MPa have been determined to be $C_{p,m}^{\circ} = 185.66 \pm 1.86 \text{ J K}^{-1} \text{ mol}^{-1}$, $S_m^{\circ} = 176.72 \pm 1.77 \text{ J K}^{-1} \text{ mol}^{-1}$ and $H_m^{\circ} = 278.41 \pm 2.78 \text{ kJ mol}^{-1}$ for D-ribose, and $C_{p,m}^{\circ} = 223.44 \pm 2.23 \text{ J K}^{-1} \text{ mol}^{-1}$, $S_m^{\circ} = 216.53 \pm 2.17 \text{ J K}^{-1} \text{ mol}^{-1}$ and $H_m^{\circ} = 339.39 \pm 3.39 \text{ kJ mol}^{-1}$ for D-mannose.

$$S_m^{\circ}(T) = \int_0^T \frac{C_p(T)}{T} dT \quad (4)$$

$$\frac{\Delta T_0^{\circ}(T)}{T} = \frac{\int_0^T C_p(T) dT}{T} \quad (5)$$

Comparison to previous results

Torres et al. performed heat capacity measurements in 2009 on D-ribose and D-mannose in the temperature range from 288.15 to 358.15 K using a power-compensation differential scanning calorimeter [25]. Also, Kawaizumi et al. determined the heat capacities of these two compounds using a laboratory-constructed isoperibol twin calorimeter of dry shield type at room temperature as early as 1981 [26]. These previous data have been plotted in Fig. 9 to compare with our measured data. It can be seen that the deviations of our D-

Table 5 Standard thermodynamic functions of D-ribose and D-mannose as a function of temperature T at the standard pressure $p^\circ = 0.1$ MPa

T/K	D-ribose			T/K	D-mannose		
	$C_{p,m}^\circ/J \text{ mol}^{-1} \text{ K}^{-1}$	$\Delta_0^T S_m^\circ/J \text{ mol}^{-1} \text{ K}^{-1}$	$\Delta_0^T H_m^\circ/kJ \text{ mol}^{-1}$		$C_{p,m}^\circ/J \text{ mol}^{-1} \text{ K}^{-1}$	$\Delta_0^T S_m^\circ/J \text{ mol}^{-1} \text{ K}^{-1}$	$\Delta_0^T H_m^\circ/kJ \text{ mol}^{-1}$
0	0	0	0	0	0	0	0
1	1.0588E-03	5.6142E-04	3.4277E-07	1	1.5165E-03	1.0632E-03	5.8789E-07
2	6.6694E-03	2.6268E-03	3.6304E-06	2	7.3718E-03	3.5274E-03	4.4644E-06
3	2.1782E-02	7.7799E-03	1.6840E-05	3	2.3219E-02	9.0608E-03	1.8635E-05
4	5.2144E-02	1.7764E-02	5.2264E-05	4	5.7101E-02	1.9832E-02	5.6879E-05
5	1.0470E-01	3.4560E-02	1.2851E-04	5	1.2006E-01	3.8678E-02	1.4249E-04
6	1.8798E-01	6.0470E-02	2.7188E-04	6	2.2602E-01	6.9164E-02	3.1131E-04
7	3.1528E-01	9.8336E-02	5.1915E-04	7	3.9075E-01	1.1552E-01	6.1412E-04
8	4.9808E-01	1.5169E-01	9.2077E-04	8	6.2961E-01	1.8239E-01	1.1176E-03
9	7.4482E-01	2.2395E-01	1.5367E-03	9	9.5392E-01	2.7440E-01	1.9019E-03
10	1.0594	3.1810E-01	2.4331E-03	10	1.3580	3.9520E-01	3.0520E-03
15	3.6057	1.1779	1.3463E-02	15	4.4742	1.4776	1.6923E-02
20	7.3196	2.7047	4.0445E-02	20	8.8895	3.3480	4.9960E-02
25	11.512	4.7846	8.7438E-02	25	13.881	5.8620	1.0676E-01
30	15.766	7.2601	1.5565E-01	30	19.056	8.8488	1.8906E-01
35	19.953	10.006	2.4498E-01	35	24.302	12.180	2.9743E-01
40	24.061	12.939	3.5505E-01	40	29.563	15.769	4.3211E-01
45	28.041	16.005	4.8538E-01	45	34.700	19.549	5.9286E-01
50	31.792	19.156	6.3508E-01	50	39.524	23.458	7.7858E-01
55	35.343	22.352	8.0288E-01	55	44.095	27.438	9.8754E-01
60	38.886	25.580	9.8849E-01	60	48.649	31.471	1.2195
65	42.343	28.829	1.1916	65	53.054	35.540	1.4738
70	45.741	32.092	1.4118	70	57.341	39.629	1.7498
75	49.101	35.362	1.6489	75	61.529	43.729	2.0470
80	52.429	38.638	1.9028	80	65.637	47.831	2.3650
85	55.731	41.915	2.1732	85	69.675	51.932	2.7033
90	59.006	45.194	2.4600	90	73.649	56.027	3.0616
95	62.254	48.471	2.7632	95	77.565	60.115	3.4397
100	65.471	51.746	3.0825	100	81.427	64.192	3.8372
110	71.811	58.285	3.7691	110	88.999	72.309	4.6895
120	78.023	64.800	4.5183	120	96.391	80.371	5.6166
130	84.112	71.287	5.3291	130	103.63	88.373	6.6168
140	90.094	77.740	6.2002	140	110.73	96.313	7.6887
150	95.991	84.157	7.1307	150	117.74	104.19	8.8311
160	101.83	90.539	8.1198	160	124.67	112.01	10.043
170	107.62	96.886	9.1671	170	131.56	119.78	11.324
180	113.40	103.20	10.272	180	138.42	127.49	12.674
190	119.19	109.49	11.435	190	145.28	135.16	14.093
200	125.00	115.75	12.656	200	152.16	142.79	15.580
210	130.85	121.99	13.935	210	159.07	150.38	17.136
220	136.75	128.21	15.273	220	166.03	157.94	18.762
230	142.73	134.42	16.671	230	173.05	165.47	20.457
240	148.78	140.62	18.128	240	180.15	172.99	22.223
250	154.92	146.82	19.646	250	187.32	180.49	24.060
260	161.16	153.02	21.227	260	194.58	187.98	25.970
270	167.50	159.22	22.870	270	201.94	195.46	27.952
273.15	169.52	161.17	23.401	273.15	204.28	197.81	28.592

Table 5 (continued)

T/K	D-ribose			T/K	D-mannose		
	$C_{p,m}^o/J \text{ mol}^{-1} \text{ K}^{-1}$	$\Delta_0^T S_m^o/J \text{ mol}^{-1} \text{ K}^{-1}$	$\Delta_0^T H_m^o/kJ \text{ mol}^{-1}$		$C_{p,m}^o/J \text{ mol}^{-1} \text{ K}^{-1}$	$\Delta_0^T S_m^o/J \text{ mol}^{-1} \text{ K}^{-1}$	$\Delta_0^T H_m^o/kJ \text{ mol}^{-1}$
280	173.96	165.43	24.577	280	209.40	202.94	30.009
290	180.53	171.65	26.349	290	216.97	210.42	32.141
298.15	185.97	176.72	27.843	298.15	223.22	216.51	33.934
300	191.57	177.88	28.188	300	233.65	217.90	34.349
305	194.86	181.07	29.154	305	237.62	221.79	35.527
310	198.94	184.27	30.138	310	241.71	225.69	36.725
315	203.46	187.49	31.144	315	245.87	229.59	37.944
320	208.56	190.73	32.174	320	250.06	233.50	39.184
325	214.87	194.01	33.231	325	254.24	237.41	40.445
330	223.54	197.36	34.326	330	258.36	241.32	41.726
335	236.20	200.81	35.473	335	262.39	245.24	43.028
340	257.87	204.45	36.702	340	266.37	249.15	44.350
345	299.79	208.48	38.082	345	270.33	253.07	45.692
350	398.75	213.39	39.790	350	274.41	256.99	47.053
355	677.43	220.67	42.359	355	278.80	260.91	48.436
360	1447.1	234.73	47.388	360	283.75	264.84	49.842
365	2482.5	262.65	57.517	365	289.64	268.80	51.275
370	1030.6	289.77	67.475	370	296.93	272.79	52.741
375	458.67	298.14	70.589	375	306.23	276.83	54.248
380	392.83	303.64	72.665	380	318.26	280.96	55.808
385	385.96	308.72	74.609	385	338.98	285.24	57.445
390	384.12	313.69	76.533	390	378.31	289.84	59.228
395	385.04	318.59	78.455	395	461.05	295.11	61.297
400	387.24	323.44	80.385	400	675.50	302.03	64.046
405	389.86	328.27	82.328	405	1324.0	313.71	68.753
410	392.49	333.07	84.284	410	2801.3	338.19	78.735
415	395.10	337.84	86.253	415	1695.9	371.49	92.466
420	397.83	342.59	88.235	420	509.79	381.55	96.661
425	400.85	347.31	90.231	425	488.13	387.35	99.109
430	404.28	352.02	92.244	430	490.58	393.07	101.56
435	407.96	356.72	94.275	435	495.12	398.77	104.02
440	411.39	361.40	96.323	440	501.76	404.46	106.51

All calculated thermodynamic values have an estimated standard uncertainty of about $0.025 \times$ below 300 K, and $0.03 \times$ above 300 K

ribose DSC data are within about -0.01 and 3% from the data of Torres and Kawaizumi, respectively, indicating that our data agree well with these previous results. For D-mannose, our PPMS data deviate from Kawaizumi's data to be about 4% . However, the DSC data from Torres are not smoothed below 303 K, and the deviations of their data above 303 K from our DSC data are within about 7% .

It should be pointed out that, as far as we know, the thermodynamic properties of the melting transition have not been reported for D-ribose and D-mannose, except that

Goldberg and Tewari [15] indicated their melting temperature to be 360 and 406 K for D-ribose and D-mannose, respectively. These melting temperatures are in rough agreement with our DSC onset temperature of 355.27 and 403.09 K. However, we could not find the related report on the melting transition enthalpy for these two compounds in previous literatures.

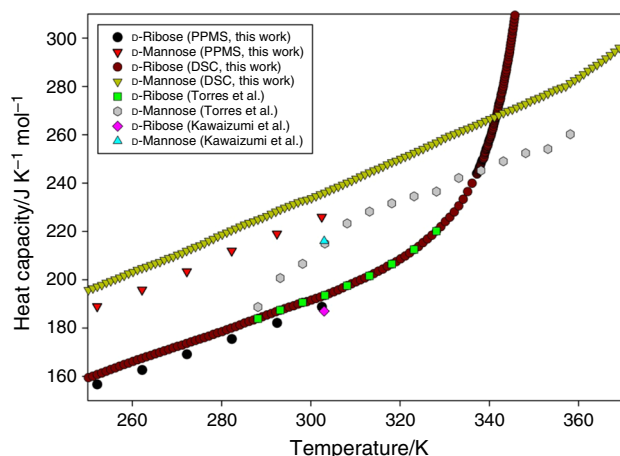


Fig. 9 Comparison of measured heat capacities in this work from those reported in literature

Conclusions

In summary, the heat capacities of D-ribose and D-mannose have been measured in the temperature range from 1.9 to 440 K using a combination of PPMS and DSC calorimeter, and the thermodynamic functions of these two compounds have been calculated based on the fitting parameters as well as the theoretical and empirical models used in the heat capacity data fitting. The standard molar heat capacity, entropy and enthalpy at 298.15 K and 0.1 MPa have been determined to be $C_{p,m}^{\circ} = 185.66 \pm 1.86 \text{ J K}^{-1} \text{ mol}^{-1}$, $S_m^{\circ} = 176.72 \pm 1.77 \text{ J K}^{-1} \text{ mol}^{-1}$ and $H_m^{\circ} = 278.41 \pm 2.78 \text{ kJ mol}^{-1}$ for D-ribose, and $C_{p,m}^{\circ} = 223.44 \pm 2.23 \text{ J K}^{-1} \text{ mol}^{-1}$, $S_m^{\circ} = 216.53 \pm 2.17 \text{ J K}^{-1} \text{ mol}^{-1}$ and $H_m^{\circ} = 339.39 \pm 3.39 \text{ kJ mol}^{-1}$ for D-mannose. Also, using the DSC heat flows, the melting onset temperature, peak temperature and transition enthalpy have been determined to be 355.27, 366.23 and 26.02 kJ mol⁻¹ for D-ribose, and 403.09, 412.26 and 26.41 kJ mol⁻¹ for D-mannose.

Acknowledgements The authors gratefully acknowledge the National Natural Science Foundation of China under Grant 21473198 and 21373215, Liaoning Provincial Natural Science Foundation of China under Grant 201602741. Q. Shi would like to thank Hundred-Talent Program founded by Chinese Academy of Sciences. S. Wang and X. Wang would like to thank the support from Research Project of Teaching Reform of Postgraduate Education in Liaoning Province (2017) and Dalian Jiaotong University Graduate Education and Teaching Reform Project (2016–10).

References

- Galema SA, Blandamer MJ, Engberts JBFN. Stereochemical aspects of hydration of carbohydrates in aqueous-solutions. 2. kinetic medium effects. *J Org Chem.* 1992;57(7):1995–2001.
- Ravindranathan KP, Gallicchio E, Levy RM. Conformational equilibria and free energy profiles for the allosteric transition of the ribose-binding protein. *J Mol Biol.* 2005;353(1):196–210.
- Tan T-C, Alkarkhi Abbas FM, Easa AM. Ribose-induced Maillard reaction as a quality index in frozen minced chicken and pork meats. *J Food Qual.* 2013;36(5):351–60.
- Taguchi T, Miwa I, Mizutani T, Nakajima H, Fukumura Y, Kobayashi I, Yabuuchi M, Miwa I. Determination of D-mannose in plasma by HPLC. *Clin Chem.* 2003;49(1):181–3.
- Parichita Mazumder, Chaitali Mukhopadhyay. Conformations, dynamics and interactions of di-, tri- and pentamannoside with mannose binding lectin: a molecular dynamics study. *Carbohydr Res.* 2012;349:59–72.
- Zhang XR, Li YX, Ding N, Guan HS. Synthesis of divalent and trivalent cluster mannosides. *Chin J Org Chem.* 2003;23(6):559–62.
- Lambrech MJ, Brichacek M, Barkauskaite E, Ariza A, Ahel I, Hergenrother PJ. Synthesis of Dimeric ADP-Ribose and Its Structure with Human Poly(ADP-ribose) Glycohydrolase. *J Am Chem Soc.* 2015;137(10):3558–64.
- Zhao Y, Yang L-X, Liu Q, Wang J-J. Volumetric properties for the electrolyte (NaCl, NaBr and NaI)-monosaccharide (D-mannose and D-ribose)-water systems at 298.15 K. *J Chin Chem Soc.* 2006;53(4):961–70.
- Ullrich O, Diestel A, Eyupoglu IY, Nitsch R. Regulation of microglial expression of integrins by poly(ADP-ribose) polymerase-1. *Nat Cell Biol.* 2001;3(12):1035–42.
- Worthley DL, Bardy PG, Mullighan CG. Mannose-binding lectin: biology and clinical implications. *Intern Med J.* 2005;35(9):548–55.
- Caldecott KW. Ribose-an internal threat to DNA. *Science.* 2014;343(6168):260–1.
- Wilhoit RC. Enthalpies of formation of sugars and sugar hydrates derived from heats of combustion. Abstracts of Papers of the American Chemical Society. 1972;18.
- Colbert JC, Domalski ES, Coxon B. Enthalpies of combustion of D-ribose and 2-deoxy-D-ribose. *J Chem Thermodyn.* 1987;19(4):433–41.
- Banipal PK, Banipal TS, Lark BS, Ahluwalia JC. Partial molar heat capacities and volumes of some mono-, di- and tri-saccharides in water at 298.15, 308.15 and 318.15 K. *J Chem Soci-Fara Trans.* 1997;93(1):81–7.
- Goldberg RN, Tewari YB. Thermodynamic and transport-properties of carbohydrates and their monophosphates—the pentoses and hexoses. *J Phys Chem Ref Data.* 1989;18(2):809–80.
- Galema SA, Engberts JBFN, Hoiland H, Forland GM. Informative thermodynamic properties of the effect of stereochemistry on carbohydrate hydration. *J Phys Chem.* 1993;97(26):6885–9.
- Alberty RA. Thermodynamic properties of nucleotide reductase reactions. *Biochemistry.* 2004;43(30):9840–5.
- Ruxi Dai, Shihui Zhang, Nan Yin, Zhi-Cheng Tan, Quan Shi. Low-temperature heat capacity and standard thermodynamic functions of beta-D-(-)-arabinose (C₅H₁₀O₅). *J Chem Thermodyn.* 2016;92:60–5.
- Tae-Jin Park, Alexandra Navrotsky. Thermochemistry and crystallization of glass-forming Y-substituted Sr-analogues of fresnoite (Sr₂TiSi₂O₈). *J Am Ceram Soc.* 2010;93(7):2055–61.
- Park T-J, Davis MJ, Vullo P, Nenoff TM, Krumhansl JL, Navrotsky A. Thermochemistry and Aqueous Durability of Ternary Glass Forming Ba-Titanosilicates: Fresnoite (Ba₂TiSi₂O₈) and Ba-Titanite (BaTiSiO₅). *J Am Ceram Soc.* 2009;92(9):2053–8.
- Lashley JC, Hundley MF, Migliori A, Sarrao JL, Pagliuso PG, Darling TW, Jaime M, Cooley JC, Hults WL, Morales L, Thoma DJ, Smith JL, Boerio-Goates J, Woodfield BF, Stewart GR, Fisher RA, Phillips NE. Critical examination of heat capacity measurements made on a quantum design physical property measurement system. *Cryogenics.* 2003;43(6):369–78.

22. Ribeiro da Silva Manuel AV, Ribeiro da Silva Maria v, Lobo Ferreira Ana IMC, Shi Q, Woodfield BF, Goldberg RN. Thermochemistry of alpha-D-xylose(cr). *J Chem Thermodyn.* 2013;58:20–8.
23. Woodfield BF, Shapiro JL, Stevens R, Boerio-Goates J. Molar heat capacity and thermodynamic functions for CaTiO₃. *J Chem Thermodyn.* 1999;31(12):1573–83.
24. Hernandez-Segura GO, Campos M, Costas M, Torres LA. Temperature dependence of the heat capacities in the solid state of 18 mono-, di-, and poly-saccharides. *J Chem Thermodyn.* 2009;41(1):17–20.
25. Kawaizumi F, Kushida S, Miyahara Y. Determination of the specific-heat capacities of aqueous-solutions of pentose. *Bull Chem Soc Jpn.* 1981;54(8):2282–5.